IJIE

UTHM Penerbit
Universiti Tun Hussein Onn Malaysia

INTERNATIONAL JOURNAL OF INTEGRATED ENGINEERING
ISSN: 2229-838X e-ISSN: 2600-7916

Vol. 18 No. 4 (2026) 139-156
https://publisher.uthm.edu.my/ojs/index.php/ijie

Boundary Element Analysis of Acoustic Wave Problems in Functionally Graded Materials

Khaeruddin Khaeruddin[1,2], Firman Firman[1,2], Muh. Nur[1,2], Eliza M. Yusup[3], Mohamad Nur Hidayat Mat[4], Mohammad Ivan Azis[1,2], Shahrul Azmir Osman[3]*

[1] *Department of Mathematics, Hasanuddin University, Makassar, INDONESIA*
[2] *Functionally Graded Materials Research Group, Hasanuddin University, Makassar, INDONESIA*
[3] *Faculty of Mechanical and Manufacturing Engineering, Universiti Tun Hussein Onn Malaysia, 86400 Parit Raja, Johor, MALAYSIA*
[4] *Faculty of Mechanical and Automotive Engineering Technology, Universiti Malaysia Pahang Al-Sultan Abdullah, Pekan, Pahang, 26600, MALAYSIA*

*Corresponding Author: shahrula@uthm.edu.my
DOI: https://doi.org/10.30880/ijie.2026.18.04.010

Article Info

Received: 25 September 2025
Accepted: 17 March 2026
Available online: 17 June 2026

Keywords

Anisotropic functionally graded materials, variable coefficients, Helmholtz-type equation, Laplace Transform, domain-boundary element method

Abstract

A combined Laplace Transform (LT) and domain-boundary element method (DBEM) was utilized to obtain numerical solutions for a spatio-temporal coefficient Helmholtz-type equation with arbitrary initial conditions and source terms, addressing acoustic wave problems in functionally graded materials (FGMs). The procedure begins by transforming the equation of the time-space variable coefficients into one of the time-variable coefficients. The equation was then converted into an integral equation using the Gaussian divergence theorem. The time variable of the integral equation is reduced by utilizing LT and its convolution theorem to obtain a domain-boundary integral equation. Numerical solutions within the LT framework were then obtained using the standard domain-boundary element method. These numerical solutions were inverted using the Stehfest method to obtain solutions for the original time variable. Several problems involving trigonometric, exponential, and quadratic spatial gradation function coefficients were solved. The numerical validation demonstrates exceptional accuracy with mean absolute relative errors as low as E = 0.001138 for quadratic gradation materials (Ns=10, Nc=32), E = 0.003411 for exponential gradation materials (Ns=8, Nc=32), and E = 0.004279 for trigonometric gradation materials (Ns=8, Nc=16). Computational efficiency analysis reveals optimal performance parameters, with relative CPU times ranging from 0.302452s to 1.93548s depending on the gradation type and discretization parameters. The validity of the analysis used to derive the domain boundary integral equations was verified, and accurate DBEM solutions were obtained. This study successfully extends the LT-DBEM approach to handle arbitrary source terms and initial conditions in variable coefficient problems, providing a robust and computationally efficient method for analyzing acoustic wave propagation in diverse functionally graded material configurations with superior accuracy compared to traditional approaches.

1. Introduction

Modeling and simulation are cost-effective and time-efficient research methods that can provide fairly accurate problem solutions (see, for example, [1-7]. However, their application is limited due to the assumptions on which the models are based. Therefore, expanding or refining the models is always necessary to cover specific cases so that the models become more flexible.

The Helmholtz equation plays a significant role in the modeling of functionally graded materials (FGMs), particularly in contexts where wave propagation, acoustics, and vibrations are of interest. **Recent advances in FGM modeling have demonstrated various approaches: topology optimization for graded damping materials to minimize sound pressure under harmonic excitation [8], semi-analytical methods for vibro-acoustic analysis of functionally graded shells in fluid environments [9], and power series solutions for wave equations in FGM cylindrical structures [10]. The Helmholtz equation is also crucial for modeling thermoacoustic effects in FGMs, where temperature gradients significantly affect acoustic wave propagation. This application is particularly important in high-temperature environments such as gas turbines and combustion chambers, where thermoacoustic systems enable energy conversion between thermal and mechanical energy [11-13]. Thermoacoustic engines and converters are designed to convert heat into acoustic energy, and vice versa, with applications in energy harvesting and low-grade heat recovery. Thermoacoustic engines rely on the structural properties of porous materials and the geometric features for optimal thermodynamic performance.

Various numerical methods have been developed to solve FGM problems governed by the Helmholtz equation. Notably, Laplace Transform combined with boundary element methods has shown promise for unsteady Helmholtz-type equations in anisotropic FGMs [14], while dual reciprocity and local semi-analytical meshless methods have been evaluated for their computational accuracy [15].

Several other recent studies have involved the modeling and simulation of various steady and unsteady problems in heterogeneous and anisotropic materials, governed by different types of equations. Several studies conducted during the last decade, such as those in [16, 17, 18, 19, 20, 21, 22, 23, 24], focused on governing equations where the coefficients, representing material properties such as diffusivity/conductivity, velocity, reaction, and rate of concentration change, depended on spatial and temporal variables. Notably, the study in [16, 22, 23] focused on models using the Helmholtz-type equation as the governing equation, with coefficients dependent on spatial and temporal variables, assuming a zero-source term and initial conditions. This study aims to build on the study in [22, 23], moving from the case of spatial and temporal variable coefficients, zero source terms, and initial conditions to the case of spatial and temporal variable coefficients, arbitrary source terms, and initial conditions.

2. The Problem Statements

2.1 Research Gap and Problem Identification

Despite significant advances in modelling functionally graded materials (FGMs), existing computational approaches for acoustic wave problems face several critical limitations that restrict their practical applicability:

1. **Limited Source Term Handling**
   Most current methods for variable coefficient Helmholtz equations are restricted to problems with zero or simplified source terms, which is unrealistic for practical acoustic applications where complex forcing functions are common.
2. **Restrictive Initial Conditions**
   Existing approaches typically assume zero or highly simplified initial conditions, failing to address the complex initial states encountered in real-world FGM applications.
3. **Computational Inefficiency**
   Traditional time-domain methods suffer from cumulative numerical errors and computational instability when dealing with spatially and temporally variable coefficients.
4. **Limited Material Gradation Types**
   Current methods have not been comprehensively validated across diverse gradation functions (exponential, trigonometric, quadratic) that are commonly used in engineering applications.

2.2 Specific Problems Addressed in This Study

This research specifically tackles the following unresolved problems:

1. Development of a robust numerical method capable of handling arbitrary source terms q(x,t) in variable coefficient Helmholtz equations
2. Extension of existing LT-DBEM approaches to accommodate arbitrary initial conditions P(x,0) = p(x)
3. Validation of the method across multiple material gradation types with quantitative accuracy assessment
4. Optimization of computational parameters for different FGM configurations

2.3 Mathematical Problem Formulation

The study seeks solutions to the following generalized Helmholtz-type equation [23]:

$$\frac{\partial}{\partial x_i}\left[\kappa_{ij}(x,t)\frac{\partial P(x,t)}{\partial x_j}\right] + \omega^2(x,t)P(x,t) + q(x,t) = \alpha(x,t)\frac{\partial P(x,t)}{\partial t} \qquad x = (x_1, x_2), t \geq 0 \tag{1}$$

where the key challenge lies in the simultaneous presence of:

- Variable coefficients $\kappa_{ij}(x,t)$, $\omega^2(x,t)$, $\alpha(x,t)$ representing spatially and temporally varying material properties
- Arbitrary source terms q(x,t) representing complex acoustic forcing
- Arbitrary initial conditions P(x,0) = p(x) representing realistic initial acoustic states

Inside a medium Ω with a boundary $\partial\Omega$, and constrained by conditions $P(x,0) = p(x)$ and either $P(x,t)$ or the flux:

$$F(x,t) = \kappa_{ij}(x,t)\frac{\partial P(x,t)}{\partial x_i}n_j \tag{2}$$

is specified. The variable coefficients $\kappa_{ij}(x,t)$, $\omega^2(x,t)$, and $\alpha(x,t)$ denote the diffusivity, reaction coefficient, and change rate, respectively, which vary both spatially and temporally to represent the functionally graded nature of the material. The source term q(x,t) represents external acoustic forcing that varies in both space and time, while the vector $n = (n_1,n_2)$ represents the outward-pointing normal to $\partial\Omega$. The anisotropic diffusivity tensor $[\kappa_{ij}]$ (i,j = 1,2) is a real symmetrical matrix with positive determinant ensuring physical realizability of the material properties (see [22]).

Also, Eq. (1) admits Einstein notation, so that Eq. (1) can be explicitly written as

$$\frac{\partial}{\partial x_1}\left(\kappa_{11}\frac{\partial P}{\partial x_1}\right) + \frac{\partial}{\partial x_1}\left(\kappa_{12}\frac{\partial P}{\partial x_2}\right) + \frac{\partial}{\partial x_2}\left(\kappa_{12}\frac{\partial P}{\partial x_1}\right) + \frac{\partial}{\partial x_2}\left(\kappa_{22}\frac{\partial P}{\partial x_2}\right) + \omega^2 P + q = \alpha\frac{\partial P}{\partial t} \tag{3}$$

2.4 Research Objectives and Expected Contributions

The primary objectives of this study are to:

1. Develop and validate a combined LT-DBEM approach that can handle both arbitrary source terms and initial conditions simultaneously.
2. Demonstrate the method's effectiveness across exponential, trigonometric, and quadratic material gradation functions.
3. Provide quantitative accuracy assessment and computational efficiency analysis.
4. Establish optimal computational parameters (Ns, Nc) for different FGM configurations.
5. Extend the applicability of numerical methods for acoustic wave problems in FGMs to more realistic engineering scenarios.

This research addresses a significant gap in the current literature by providing the first comprehensive treatment of variable coefficient Helmholtz equations with simultaneous arbitrary source terms and initial conditions, validated across multiple gradation types with rigorous error analysis.

3. The Boundary Integral Equation

The coefficients $\kappa_{ij}, \omega^2, \alpha$ are required to take the form (see [14])

$$\kappa_{ij}(x,t) = \overline{\kappa}_{ij}(t)g(x) \tag{4}$$

$$\omega^2(x,t) = \overline{\omega}^2(t)g(x) \tag{5}$$

$$\alpha(x,t) = \overline{\alpha}(t)g(x) \tag{6}$$

where the $\overline{\kappa}_{ij}, \overline{\omega}^2, \overline{\alpha}$ are time-dependent parameters and g is a differentiable function of x. Use of Eq. (4), Eq. (5) and Eq. (6) in Eq. (1) yields

$$\overline{\kappa}_{ij}\frac{\partial}{\partial x_i}\left(g\frac{\partial P}{\partial x_j}\right) + \overline{\omega}^2 gP + q = \overline{\alpha}g\frac{\partial P}{\partial t} \tag{7}$$

Adopting the transformation approach established in the literature [16, 24], we define

$$P(x,t) = g^{-1/2}(x)\psi(x,t) \tag{8}$$

Subsequently, incorporating Equations (4) and (8) into Equation (2) and applying the mathematical identity

$$g\frac{\partial g^{-1/2}}{\partial x_i} = -\frac{\partial g^{\frac{1}{2}}}{\partial x_i} \tag{9}$$

Gives ([22])

$$F(x,t) = -F_g(x,t)\psi(x,t) + g^{1/2}(x)F_\psi(x,t) \tag{10}$$

where see ([22])

$$F_g(x,t) = \overline{\kappa}_{ij}(t)\frac{\partial g^{1/2}(x)}{\partial x_j}n_i(x) \qquad F_\psi(x,t) = \overline{\kappa}_{ij}(t)\frac{\partial \psi(x,t)}{\partial x_j}n_i(x)$$

Following the analysis in [24], Eq. (7) can be written as

$$g^{1/2}\overline{\kappa}_{ij}\frac{\partial^2\psi}{\partial x_i\partial x_j} - \psi\overline{\kappa}_{ij}\frac{\partial^2 g^{1/2}}{\partial x_i\partial x_j} + \overline{\omega}^2 g^{1/2}\psi + q = \overline{\alpha}g^{1/2}\frac{\partial\psi}{\partial t}$$

It follows (see [22]) that if g is such that

$$\overline{\kappa}_{ij}(t)\frac{\partial^2 g^{1/2}(x)}{\partial x_i\partial x_j} - \lambda(t)g^{1/2}(x) = 0 \tag{11}$$

where λ is a parameter (see [22]), then the variable coefficients equation (7) becomes (see [22])

$$\overline{\kappa}_{ij}\frac{\partial^2\psi}{\partial x_i\partial x_j} + \left(\overline{\omega}^2 - \lambda\right)\psi + qg^{-1/2} = \overline{\alpha}\frac{\partial\psi}{\partial t} \tag{12}$$

By multiplying Equation (12) by the weighting function $\Phi(x,t|x_0,\bar{t})$ and subsequently performing integration across both temporal and spatial domains [22], we obtain

$$\int_0^t\int_\Omega\left[\overline{\kappa}_{ij}\frac{\partial^2\psi}{\partial x_i\partial x_j} + \left(\overline{\omega}^2 - \lambda\right)\psi + qg^{-1/2} - \overline{\alpha}\frac{\partial\psi}{\partial t}\right]\Phi\, dx_0\, d\bar{t} = 0 \tag{13}$$

Application of the Gauss divergence theorem in two successive steps to evaluate the integral [24] $\int_0^t\int_\Omega \overline{\kappa}_{ij}\frac{\partial^2\psi}{\partial x_i\partial x_j}\Phi\, dx_0\, d\bar{t}$ within Equation (13) leads to

$$\int_0^t\int_\Omega \overline{\kappa}_{ij}\frac{\partial^2\psi}{\partial x_i\partial x_j}\Phi\, dx_0\, d\bar{t} = \int_0^t\int_{\partial\Omega} F_\psi\Phi\, dx_0\, d\bar{t} - \int_0^t\int_\Omega \overline{\kappa}_{ij}\frac{\partial\psi}{\partial x_i}\frac{\partial\Phi}{\partial x_j}\, dx_0\, d\bar{t}$$
$$= \int_0^t\int_{\partial\Omega}\left(F_\psi\Phi - \psi\Gamma\right)dx_0\, d\bar{t} + \int_0^t\int_\Omega \psi\overline{\kappa}_{ij}\frac{\partial^2\Phi}{\partial x_i\partial x_j}\, dx_0\, d\bar{t}$$

where $\Gamma = \overline{\kappa}_{ij} \frac{\partial \Phi}{\partial x_j} n_i$. Therefore Eq. (13) becomes

$$\int_0^t \int_{\partial\Omega} \left(F_\psi \Phi - \psi\Gamma\right) dx_0 \, d\bar{t} + \int_0^t \int_\Omega \left[\overline{\kappa}_{ij} \frac{\partial^2 \Phi}{\partial x_i \partial x_j} + \left(\overline{\omega}^2 - \lambda\right)\Phi\right] \psi \, dx_0 \, d\bar{t} + \int_0^t \int_\Omega \left[q g^{-1/2} - \overline{\alpha} \frac{\partial \psi}{\partial t}\right] \Phi \, dx_0 \, d\bar{t} = 0 \tag{14}$$

Substituting Eq. (10) for F_ψ and Eq. (8) for ψ in Eq. (14)

$$\int_{\partial\Omega} \int_0^t \left[\left(F g^{-1/2} + F_g P\right)\Phi - P g^{1/2} \Gamma\right] d\bar{t} \, dx_0 + \int_\Omega g^{1/2} \int_0^t \left\{\overline{\kappa}_{ij} \frac{\partial^2 \Phi}{\partial x_i \partial x_j} P + \left[\left(\overline{\omega}^2 - \lambda\right) P - \overline{\alpha} \frac{\partial P}{\partial t}\right] \Phi\right\} d\bar{t} \, dx_0 + \int_\Omega \int_0^t q g^{-1/2} \Phi \, d\bar{t} \, dx_0 = 0 \tag{15}$$

Applying the LT and its convolution theorem to the time integral in Eq. (15) yields (see[24])

$$\int_{\partial\Omega} \left[\left(F^* g^{-1/2} + F_g^* P^*\right)\Phi - P^* g^{1/2} \Gamma^*\right] dx_0 + \int_\Omega g^{1/2} \left[\overline{\kappa}_{ij}^* \frac{\partial^2 \Phi^*}{\partial x_i \partial x_j} + \left(\overline{\omega}^{*2} - \lambda^* - s\overline{\alpha}^*\right)\Phi^*\right] P^* \, dx_0 + \int_\Omega \left(q^* g^{-1/2} + g^{1/2} \overline{\alpha}^* p\right)\Phi^* dx_0 = 0 \tag{16}$$

where * denotes the LT of a function and s is the variable of LT (see [23]). If we take

$$\overline{\kappa}_{ij}^* \frac{\partial^2 \Phi^*}{\partial x_i \partial x_j} + \left(\overline{\omega}^{*2} - \lambda^* - s\overline{\alpha}^*\right)\Phi^* = \delta(x, x_0) \tag{17}$$

$$\Gamma^*(x, x_0) = \overline{\kappa}_{ij}^* \frac{\partial \Phi^*}{\partial x_j} n_i$$

where δ is the Dirac delta function and Eq. (16) can be written as

$$\eta(x) g^{1/2}(x) \mu^*(x, s) = \int_{\partial\Omega} \left\{\left[\Gamma^*(x, x_0) g^{1/2}(x_0) - \Phi^*(x, x_0) F_g^*(x_0, s)\right] P^*(x_0, s) - \Phi^*(x, x_0) g^{-1/2}(x_0) F^*(x_0, s)\right\} dx_0 - \int_\Omega \left[\overline{\alpha}^* g^{1/2}(x_0) p(x_0) + q^*(x_0, s) \, g^{-1/2}(x_0)\right] \Phi^*(x, x_0) \, dx_0 \tag{18}$$

In two-dimensional configurations, the fundamental solutions Φ^* and Γ^* [22] that satisfy Eq. (17) are given by

$$\Phi^*(x, x_0) = \begin{cases} \frac{\sigma}{2\pi} \ln R & if \ \overline{\omega}^{*2} - \lambda^* - s\overline{\alpha}^* = 0 \\ \frac{\iota\sigma}{4} H_0^{(2)}(\rho R) & if \ \overline{\omega}^{*2} - \lambda^* - s\overline{\alpha}^* > 0 \\ \frac{-\sigma}{2\pi} K_0(\rho R) & if \ \overline{\omega}^{*2} - \lambda^* - s\overline{\alpha}^* < 0 \end{cases} \tag{19}$$

$$\Gamma^*(x, x_0) = \begin{cases} \frac{\sigma}{2\pi} \frac{1}{R} \overline{\kappa}_{ij}^* \frac{\partial R}{\partial x_j} n_i & if \ \overline{\omega}^{*2} - \lambda^* - s\overline{\alpha}^* = 0 \\ \frac{-\iota\sigma\rho}{4} H_1^{(2)}(\rho R) \overline{\kappa}_{ij}^* \frac{\partial R}{\partial x_j} n_i & if \ \overline{\omega}^{*2} - \lambda^* - s\overline{\alpha}^* > 0 \\ \frac{\sigma\rho}{2\pi} K_1(\rho R) \overline{\kappa}_{ij}^* \frac{\partial R}{\partial x_j} n_i & if \ \overline{\omega}^{*2} - \lambda^* - s\overline{\alpha}^* < 0 \end{cases}$$

where (see [14])

$$\sigma = \ddot{\tau}/D$$
$$\rho = \sqrt{\left|\overline{\omega}^{*2} - \lambda^* - s\overline{\alpha}^*\right|/D}$$
$$D = \left[\overline{\kappa}_{11}^* + 2\overline{\kappa}_{12}^* \dot{\tau} + \overline{\kappa}_{22}^* (\dot{\tau}^2 + \ddot{\tau}^2)\right]/2$$
$$R = \sqrt{(\dot{x}_1 - \dot{a})^2 + (\dot{x}_2 - \dot{b})^2}$$
$$\dot{x}_1 = x_1 + \dot{\tau} x_2$$
$$\dot{a} = a + \dot{\tau} b$$

$$\dot{x}_2 = \ddot{\tau}x_2$$
$$\dot{b} = \ddot{\tau}b$$

where $\dot{\tau}$ and $\ddot{\tau}$ (see [14]) are the real and positive imaginary parts of the complex root τ of the quadratic

$$\overline{\kappa}_{11}^{*} + 2\overline{\kappa}_{12}^{*}\tau + \overline{\kappa}_{22}^{*}\tau^2 = 0$$

and $H_0^{(2)}$, $H_1^{(2)}$ denote the Hankel functions of the second kind and order zero and order one, respectively. K_0, K_1 denote the modified Bessel functions of order zero and order one, respectively, ι represents the square root of minus one. The derivatives $\partial R/\partial x_j$ needed to calculate the Γ in Eq. (19) are given by (see [14])

$$\frac{\partial R}{\partial x_1} = \frac{1}{R}(\dot{x}_1 - \dot{a})$$
$$\frac{\partial R}{\partial x_2} = \dot{\tau}\left[\frac{1}{R}(\dot{x}_1 - \dot{a})\right] + \ddot{\tau}\left[\frac{1}{R}(\dot{x}_2 - \dot{b})\right]$$

Knowing the solutions $P^*(x,s)$ and its derivatives $\partial P^*/\partial x_1$ and $\partial P^*/\partial x_2$ which are obtained from Eq. (18), the numerical LT inversion technique using the Stehfest formula is employed to determine the values of $P(x,t)$ and its derivatives $\partial P/\partial x_1$ ([14]). The Stehfest formula is

$$\begin{aligned} P(x,t) &\simeq \frac{\ln 2}{t}\sum_{m=1}^{N_s} V_m P^*(x,s_m) \\ \frac{\partial P(x,t)}{\partial x_1} &\simeq \frac{\ln 2}{t}\sum_{m=1}^{N_s} V_m \frac{\partial P^*(x,s_m)}{\partial x_1} \\ \frac{\partial P(x,t)}{\partial x_2} &\simeq \frac{\ln 2}{t}\sum_{m=1}^{N_s} V_m \frac{\partial P^*(x,s_m)}{\partial x_2} \end{aligned} \tag{20}$$

where (see [22])

$$s_m = \frac{\ln 2}{t}m$$

$$V_m = (-1)^{\frac{N_s}{2}+m}\sum_{k=\left[\frac{m+1}{2}\right]}^{\min\left(m,\frac{N_s}{2}\right)} \frac{k^{N_s/2}(2k)!}{\left(\frac{N_s}{2}-k\right)!k!(k-1)!(m-k)!(2k-m)!}$$

Possible multiparameter forms include

$$(x) = \begin{cases} if\ \ \lambda = 0 \\ \quad (c_0 + c_1x_1 + c_2x_2)^2 \\ if\ \ \lambda \neq 0 \\ \quad [A\cos(c_0 + c_1x_1 + c_2x_2) + B\sin(c_0 + c_1x_1 + c_2x_2)]^2, \overline{\kappa}_{ij}c_ic_j + \lambda = 0 \\ \quad [A\exp(c_0 + c_1x_1 + c_2x_2)]^2, \overline{\kappa}_{ij}c_ic_j - \lambda = 0 \end{cases} \tag{21}$$

where A, B, c_i are real constants.

4. Numerical Examples

Multiple benchmark problems possessing known analytical solutions were selected to assess the precision of the numerical methodology. Through the application of the boundary domain integral equation (18) combined with the Stehfest inversion formula presented in Equation (20), numerical solutions are computed for these test cases with the primary objective of confirming the validity of the analytical framework underlying the derivation of integral equation (18).

To maintain computational simplicity, all test problems are formulated within a unit square domain defined by corner points (0,0), (1,0), (1,1), and (0,1). The discretization scheme utilizes 320 uniformly distributed boundary elements, with 80 elements allocated along each edge of the square geometry. Constant element approximations are employed in conjunction with Bode's quadrature rule for evaluating the boundary integrals appearing in Equation (18). The domain integral in Eq. (18) is computed using a method for area integrals over a specified number of N_c of triangular cells. The domain mesh is illustrated in Figure 1. We developed a FORTRAN code to compute the solutions, along with a simple script embedded in the main FORTRAN code to calculate the values of the Stehfest constants $V_m, m = 1,2, \dots, N_s$ as described in Eq. (20) (see [22]). Table 1 presents the values of V_m obtained from the scripts for $N_s = 8,10,12$ (see [21, 24]).

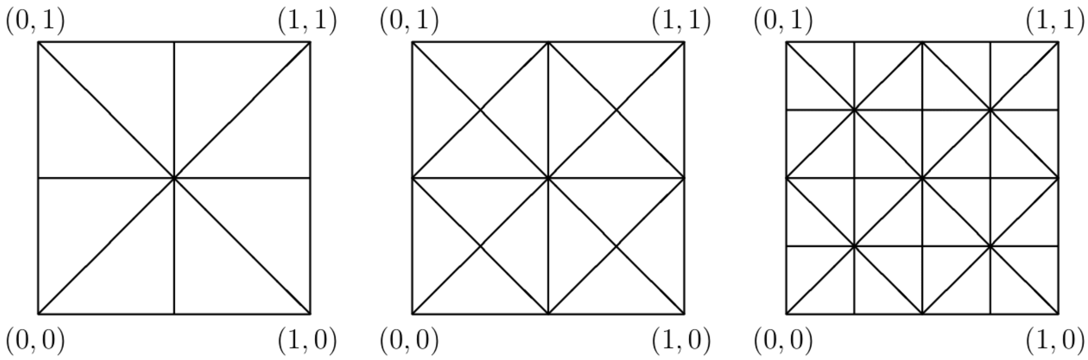

Fig. 1 *The domain mesh of triangular cells: 8 cells (left), 16 cells (middle), 32 cells (right)*

Table 1 *Values of* $\boldsymbol{V_m}$ *(see [21. 24])*

V_m	$N_s = 8$	$N_s = 10$	$N_s = 12$
V_1	$-1/3$	$1/12$	$-1/60$
V_2	$145/3$	$-385/12$	$961/60$
V_3	-906	1279	-1247
V_4	$16394/3$	$-46871/3$	$82663/3$
V_5	$-43130/3$	$505465/6$	$-1579685/6$
V_6	18730	-236957.5	1324138.7
V_7	$-35840/3$	$1127735/3$	$-58375583/15$
V_8	$8960/3$	$-1020215/3$	$21159859/3$
V_9		164062.5	-8005336.5
V_{10}		-32812.5	5552830.5
V_{11}			-2155507.2
V_{12}			359251.2

For each problem, numerical solutions $\boldsymbol{P}$ are calculated at $\boldsymbol{19 \times 19}$ interior points $(\boldsymbol{x_1}, \boldsymbol{x_2}) = \boldsymbol{X_1} \times \boldsymbol{X_2}$ where

$$\boldsymbol{X_1} = \boldsymbol{X_2} = \{\mathbf{0.05}, \mathbf{0.1}, \mathbf{0.15}, \dots, \mathbf{0.85.0.9}, \mathbf{0.95}\}$$

and 10 time-steps $\boldsymbol{t} = \{\mathbf{0.1}, \mathbf{0.2}, \mathbf{0.3}, \dots, \mathbf{0.8}, \mathbf{0.9}, \mathbf{1.0}\}$. The boundary and initial conditions are shown in Figure 2.

The absolute relative error $\boldsymbol{e}$ at a point $(\boldsymbol{x}, \boldsymbol{t})$ (see [24]) and the mean absolute relative errors $\boldsymbol{E_t}$ and $\boldsymbol{E}$ were computed using the following formulas

$$\boldsymbol{e} = |(\boldsymbol{P^n} - \boldsymbol{P^a})/\boldsymbol{P^a}|$$
$$\boldsymbol{E_t} = \frac{\mathbf{1}}{\mathbf{19 \times 19}} \sum_{\boldsymbol{i=1}}^{\mathbf{19 \times 19}} |(\boldsymbol{P_i^n} - \boldsymbol{P_i^a})/\boldsymbol{P_i^a}|$$
$$\boldsymbol{E} = \frac{\mathbf{1}}{\mathbf{19 \times 19 \times 10}} \sum_{\boldsymbol{i=1}}^{\mathbf{19 \times 19 \times 10}} |(\boldsymbol{P_i^n} - \boldsymbol{P_i^a})/\boldsymbol{P_i^a}|$$

where $\boldsymbol{P_n}$ and $\boldsymbol{P_a}$ are numerical and analytical solutions, respectively. Furthermore, we defined the relative CPU time $\boldsymbol{\theta}$ as the product of the CPU time and error $\boldsymbol{E}$ (see [22]) for every value of $\boldsymbol{N_s}$ and $\boldsymbol{N_c}$.

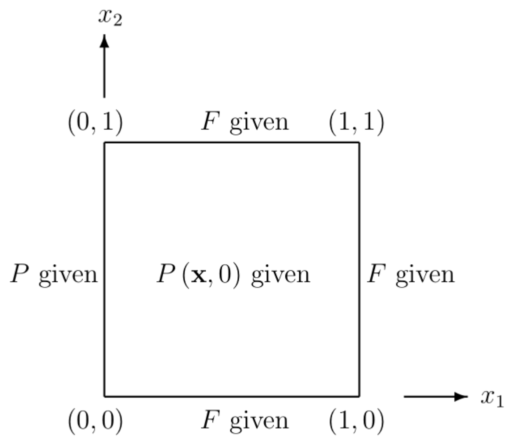

Fig. 2 *Known values on the boundary and in the domain*

Problem 1: Exponentially graded materials

First, we consider a system with coefficients and parameters as follows (see [24])

$g(x) = [\exp(0.5 + 0.1x_1 - 0.1x_2)]^2$

$\overline{\kappa}_{ij}(t) = \begin{bmatrix} 1 & 0.05 \\ 0.05 & 0.85 \end{bmatrix} \exp(-t)$

$\overline{\omega}^2(t) = \sin\sqrt{t}$

$\overline{\alpha}(t) = -0.0175(-20x_1 + 13x_2)t\exp(-t) - 1.75\exp(-t) + t\sin\sqrt{t} + 100\sin\sqrt{t} + t + 100$

$p(x) = 100(-20x_1 + 13x_2)\exp(-0.5 - 0.1x_1 + 0.1x_2)$

$q(x,t) = (t + 100)(-20x_1 + 13x_2)\exp(0.5 + 0.1x_1 - 0.1x_2)$

$\lambda(t) = 0.0175\exp(-t)$

The function $g(x)$ is shown in Figure 2. The analytical solution is

$P(x,t) = \frac{(t+100)(-20x_1+13x_2)}{\exp(0.5+0.1x_1-0.1x_2)}$

The computational findings are documented in Table 2 and Figures 4-7. Optimal accuracy with minimal computational cost was achieved using parameter combinations $N_s = 8, N_c = 32$ for error E minimization and $N_s = 8, N_c = 16$ for computational efficiency. Conversely, suboptimal performance characterized by maximum error E and computational overhead occurred with configurations $N_s = 10, N_c = 64$ and $N_s = 12, N_c = 64$ (refer to Table 2 and Figure 4). The temporal error analysis E_t displayed in Figure 5 confirms these findings, demonstrating that throughout the time interval t ∈ [0.1, 1.0], superior and inferior accuracy correspond to parameter sets $N_s = 8, N_c = 32$ and $N_s = 10, N_c = 64$, respectively. Spatial error distribution at the intermediate time t = 0.6 (Figure 6) reveals consistently lower point-wise errors e across the computational domain when employing $N_s = 8, N_c = 32$ than when $N_s = 10, N_c = 64$. The temporal evolution of errors at the central location (0.5, 0.5) shown in Figure 7 further validates the superior performance of the $N_s = 8, N_c = 32$ configuration over the $N_s = 10, N_c = 64$ alternative.

Table 2 *Values of* $\boldsymbol{E}$*and* $\boldsymbol{\theta}$ *for Problem 1*

N_s	N_c			
	16	32	64	
8	0.003537	0.003411	0.030946	E
	1.07961	1.17824	10.6372	θ (s)
10	0.00354	0.003411	0.030954	E
	1.32037	1.44401	13.4482	θ (s)
12	0.003826	0.003607	0.030882	E
	1.75362	1.67106	15.907	θ (s)

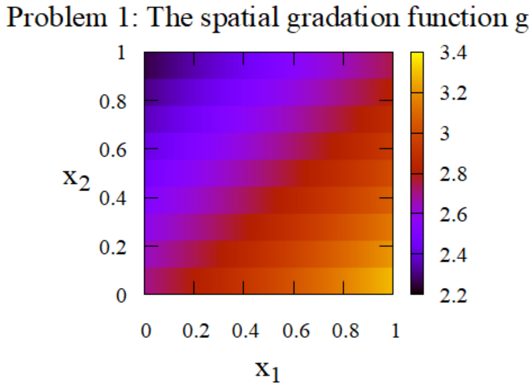

Fig. 3 *The function $g(x)$ for Problem 1*

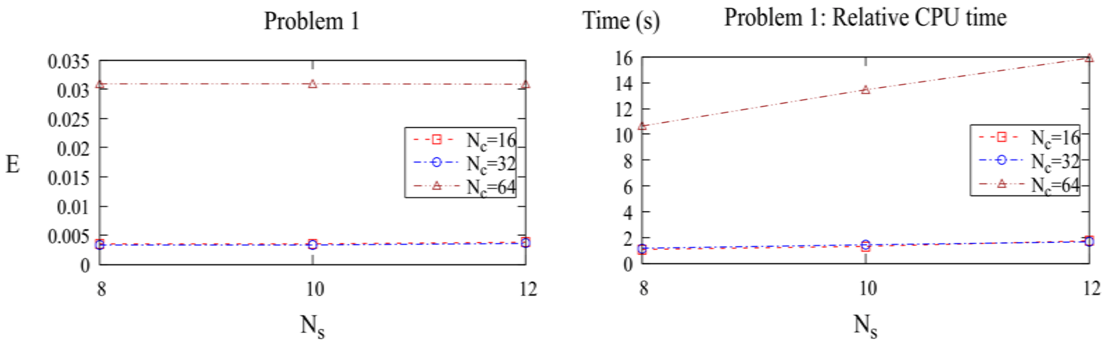

Fig. 4 *Values of E and θ for Problem 1*

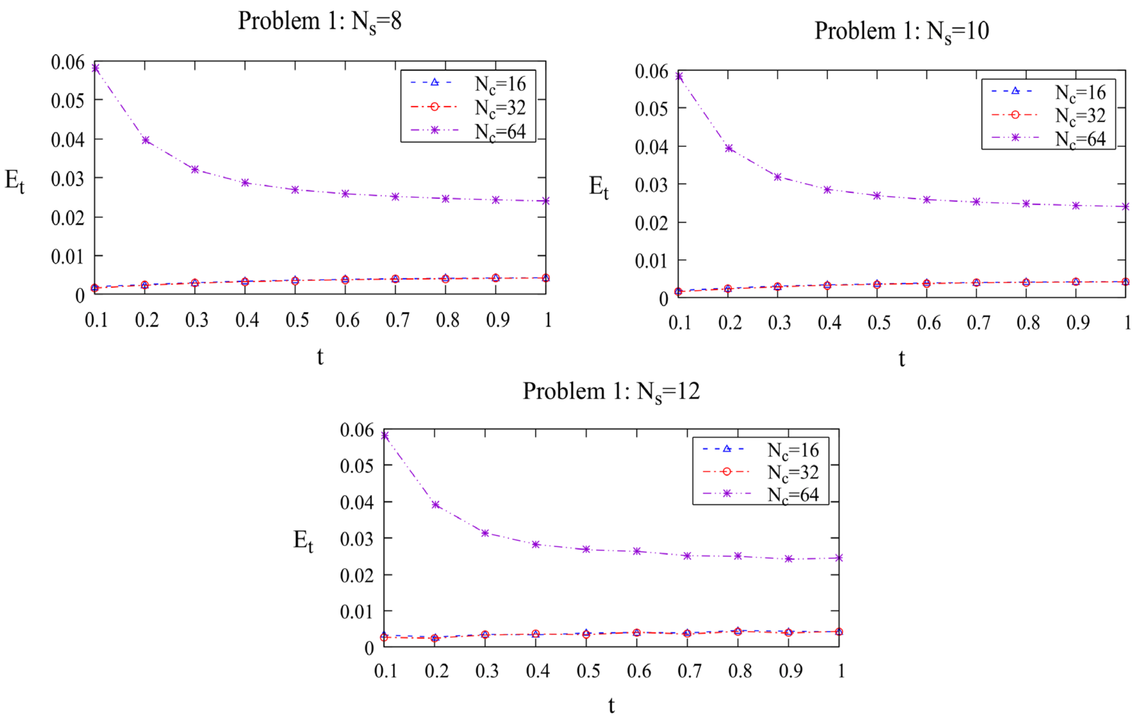

Fig. 5 *Values of E_t for Problem 1*

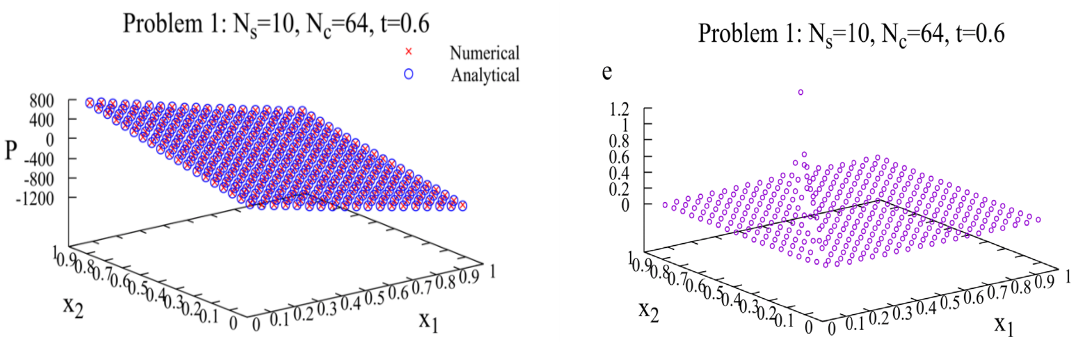

Fig. 6 *Values of* $\boldsymbol{P}$ *and* $\boldsymbol{e}$ *at* $\boldsymbol{t = 0.6}$ *for Problem 1*

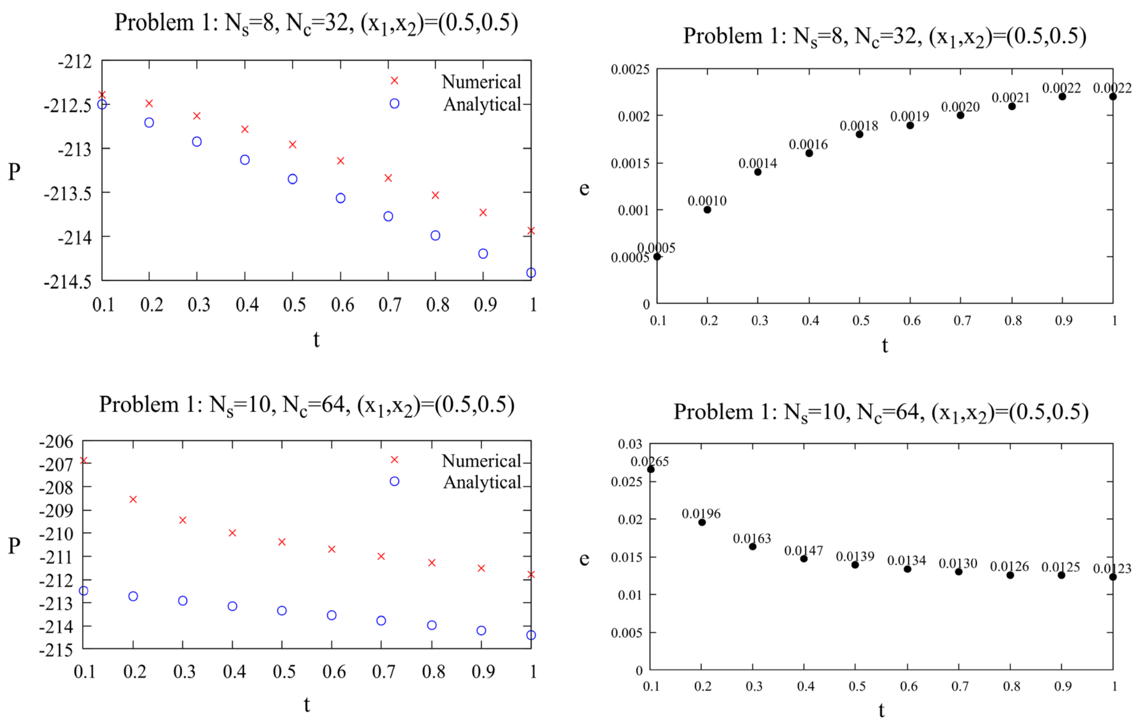

Fig. 7 *Values of* $\boldsymbol{P}$ *and* $\boldsymbol{e}$ *at* $(\boldsymbol{x_1}, \boldsymbol{x_2}) = (\boldsymbol{0.5}, \boldsymbol{0.5})$ *for Problem 1*

Problem 2: Trigonometrically graded materials

Next, we consider a system with coefficients and parameters as follows

$g(x) = [\cos(0.5 + 0.1x_1 - 0.1x_2) + \sin(0.5 + 0.1x_1 - 0.1x_2)]^2$

$\overline{\kappa}_{ij}(t) = \begin{bmatrix} 1 & 0.05 \\ 0.05 & 0.85 \end{bmatrix} \exp(-t)$

$\overline{\omega}^2(t) = \sin\sqrt{t}$

$\overline{\alpha}(t) = t\sin\sqrt{t} + 0.064t\exp(-t) + 10\sin\sqrt{t} + 0.64\exp(-t) + t + 10$

$p(x) = \frac{10\exp(-0.2x_1 + 0.1x_2)}{\cos(0.5 + 0.1x_1 - 0.1x_2) + \sin(0.5 + 0.1x_1 - 0.1x_2)}$

$(x, t) = (t + 10)\exp(-0.2x_1 + 0.1x_2)[\cos(0.5 + 0.1x_1 - 0.1x_2) + \sin(0.5 + 0.1x_1 - 0.1x_2)]$

$\lambda(t) = -0.0175\exp(-t)$

The function $g(x)$ is shown in Figure 7. The analytical solution is ([24])

$P(x, t) = \frac{(t + 10)\exp(-0.2x_1 + 0.1x_2)}{\cos(0.5 + 0.1x_1 - 0.1x_2) + \sin(0.5 + 0.1x_1 - 0.1x_2)}$

Analysis of Table 3 and Figure 9 reveals that the optimal balance between accuracy and computational efficiency is achieved with the parameter set $N_s = 8, N_c = 16$, yielding both minimum error E and reduced relative

CPU time. In contrast, degraded performance manifested through elevated error E and extended computational duration was observed for configurations $N_s = 8, N_c = 64$ and $N_s = 12, N_c = 64$. These computational trends are corroborated by the temporal error behavior E_t presented in Figure 10, which demonstrates that across the time domain $t \in [0.1, 1.0]$, the most favorable and unfavorable accuracy levels correspond to $N_s = 8, N_c = 16$ and $N_s = 8, N_c = 64$, respectively. Examination of spatial error distribution at $t = 0.6$ (Figure 11) shows consistently reduced point-wise errors e throughout the computational domain when utilizing $N_s = 8, N_c = 16$ than when $N_s = 8, N_c = 64$. The temporal error evolution at the domain center (0.5, 0.5) depicted in Figure 12 reinforces the advantage of the $N_s = 8, N_c = 16$ configuration over its $N_s = 8, N_c = 64$ counterpart.

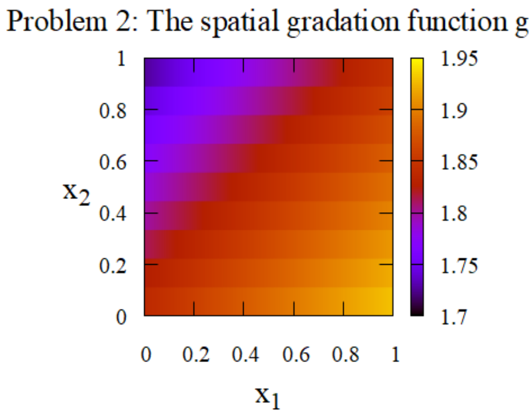

Fig. 8 *The function $g(x)$ for Problem 2*

Table 3 *Values of E and θ for Problem 2*

N_s	N_c 16	32	64	
8	0.004279	0.004312	0.009618	E
	1.71331	1.93548	4.44952	θ (s)
10	0.004288	0.004319	0.009617	E
	2.02805	2.44383	5.53562	θ (s)
12	0.004336	0.004302	0.009607	E
	2.46694	2.50226	6.52999	θ (s)

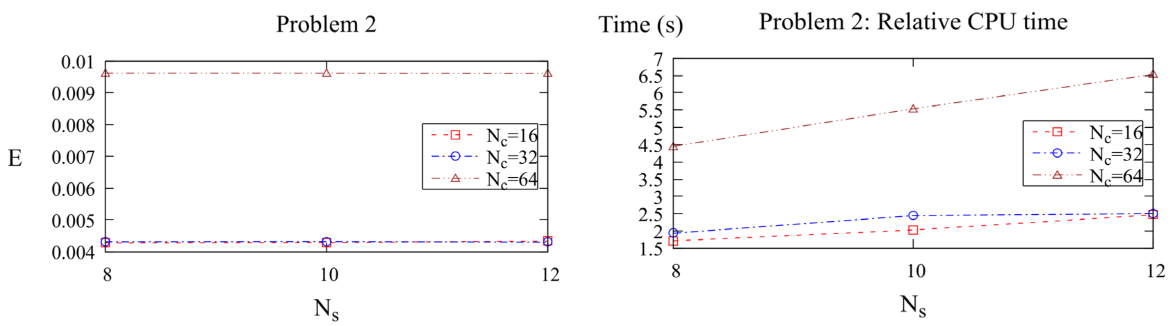

Fig. 9 *Values of E and θ for Problem 2*

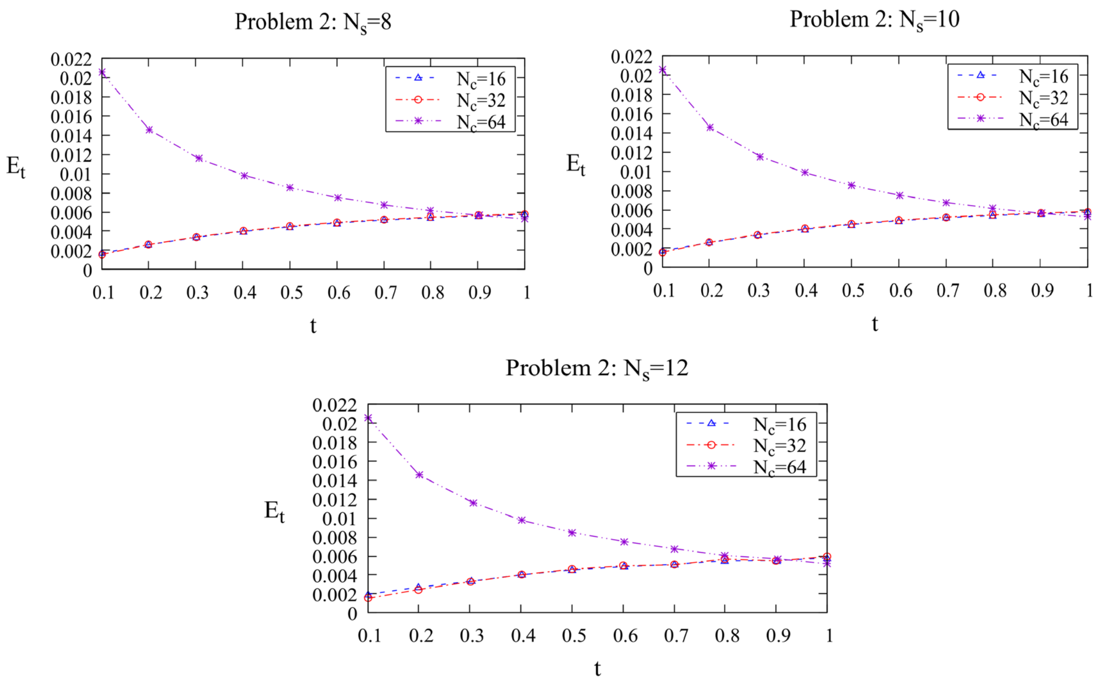

Fig. 10 *Values of E_t for Problem 2*

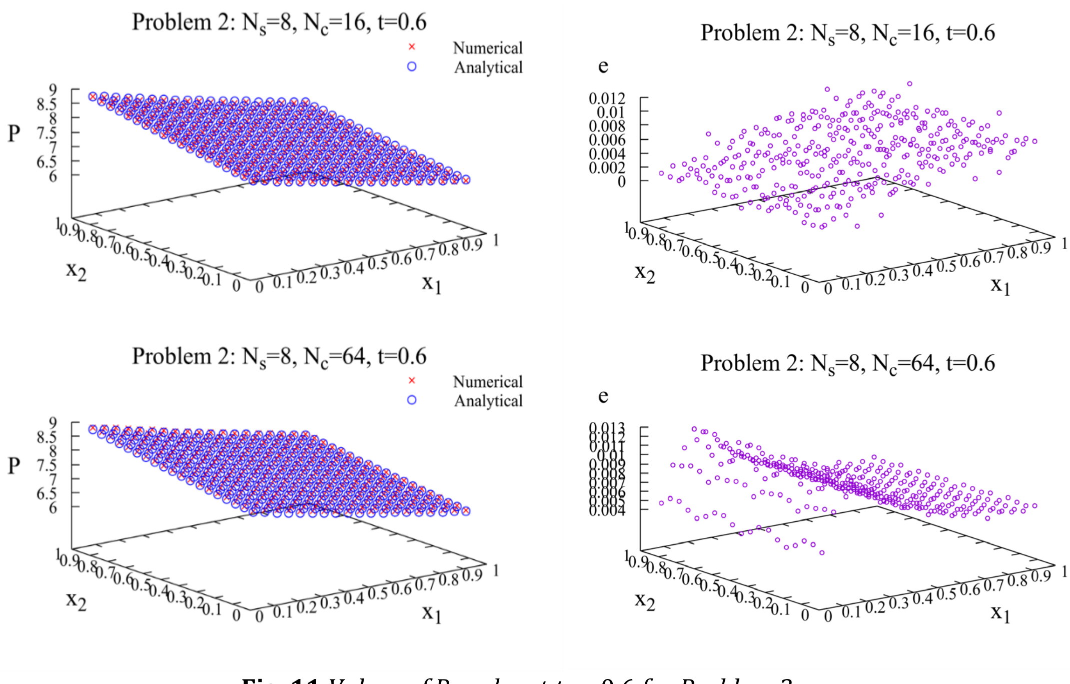

Fig. 11 *Values of P and e at $t = 0.6$ for Problem 2*

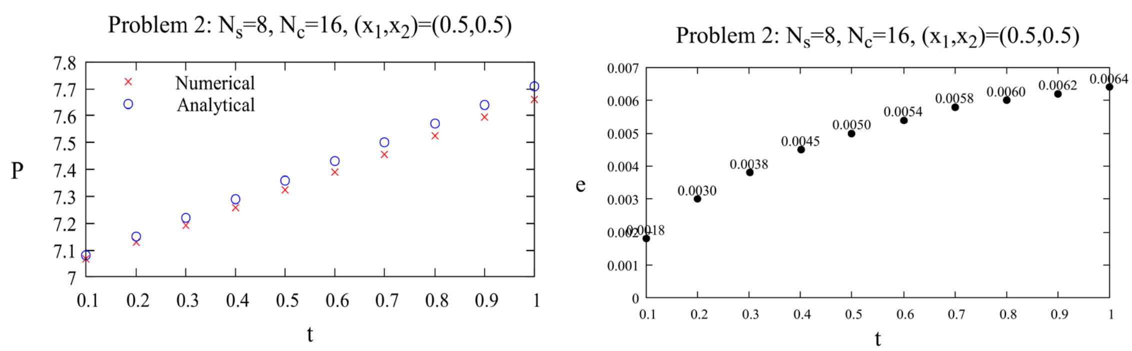

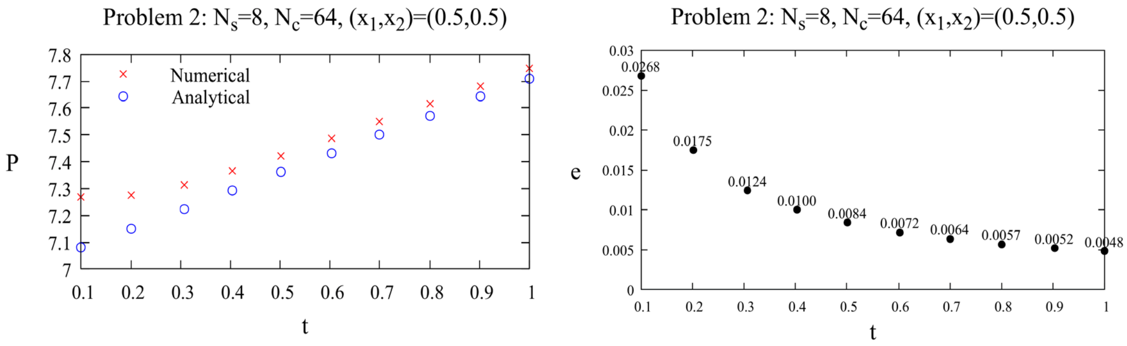

Fig. 12 *Values of P and e at* $(x_1, x_2) = (0.5,0.5)$ *for Problem 2*

Problem 3: Quadratically spatial gradation material

We now consider a system with coefficients and parameters, as follows ([24])

$g(x) = (0.5 + 0.1x_1 - 0.1x_2)^2$

$\overline{\kappa}_{ij}(t) = \begin{bmatrix} 1 & 0.05 \\ 0.05 & 0.85 \end{bmatrix} \exp(-t)$

$\overline{\omega}^2(t) = \sin\sqrt{t}$

$\overline{\alpha}(t) = -0.0005t\left[93\exp(-t) - 2000\sin\sqrt{t} - 2000\right]$

$p(x) = 0$

$q(x,t) = 10t[\cos(-0.2x_1 + 0.1x_2) + \sin(-0.2x_1 + 0.1x_2)](0.5 + 0.1x_1 - 0.1x_2)$

$\lambda(t) = 0$

The function $g(x)$ is shown in Figure 12. The analytical solution is

$$P(x,t) = \frac{10t[\cos(-0.2x_1+0.1x_2)+\sin(-0.2x_1+0.1x_2)]}{0.5+0.1x_1-0.1x_2}$$

The performance analysis summarized in Table 4 and Figure 14 demonstrates that maximum accuracy is attained with $N_s = 10, N_c = 32$, while optimal computational efficiency occurs using $N_s = 8, N_c = 32$. Conversely, the poorest accuracy and highest computational cost are associated with parameter combinations $N_s = 8, N_c = 64$ and $N_s = 12, N_c = 64$, respectively. The temporal error characteristics E_t illustrated in Figure 15 support these observations, indicating that throughout the simulation period t ∈ [0.1, 1.0], the best and worst accuracy levels are achieved with $N_s = 10, N_c = 32$ and $N_s = 8, N_c = 64$, respectively. Spatial error analysis at the representative time t = 0.6 (Figure 16) confirms that point-wise errors e across the computational domain remain consistently lower when employing $N_s = 10, N_c = 32$ compared to $N_s = 8, N_c = 64$. The temporal error progression at the central point (0.5, 0.5) shown in Figure 17 further substantiates the superior accuracy of the $N_s = 10, N_c = 32$ configuration relative to the $N_s = 8, N_c = 64$, alternative.

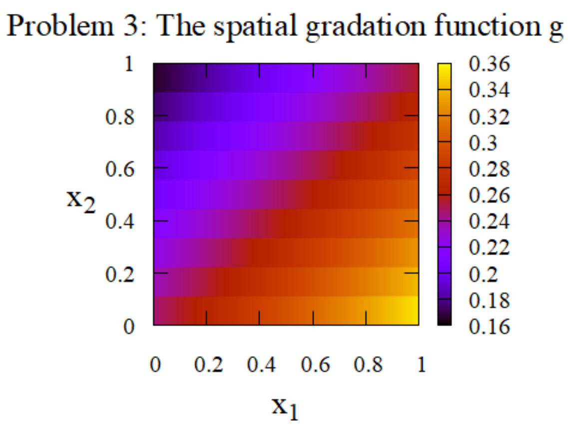

Fig. 13 *The function* $g(x)$ *for Problem 3*

Table 4 *Values of E and θ for Problem 3*

N_s	N_c 16	32	64	
8	0.003161	0.001144	0.020442	E
	0.799072	0.302452	5.97728	θ (s)
10	0.003167	0.001138	0.02031	E
	0.997669	0.406334	7.52272	θ (s)
12	0.003169	0.001142	0.02023	E
	1.18761	0.393181	8.96894	θ (s)

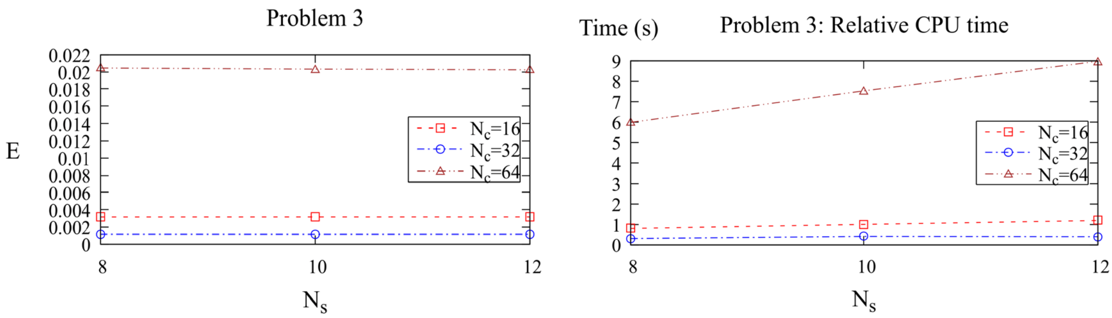

Fig. 14 *Values of E and θ for Problem 3*

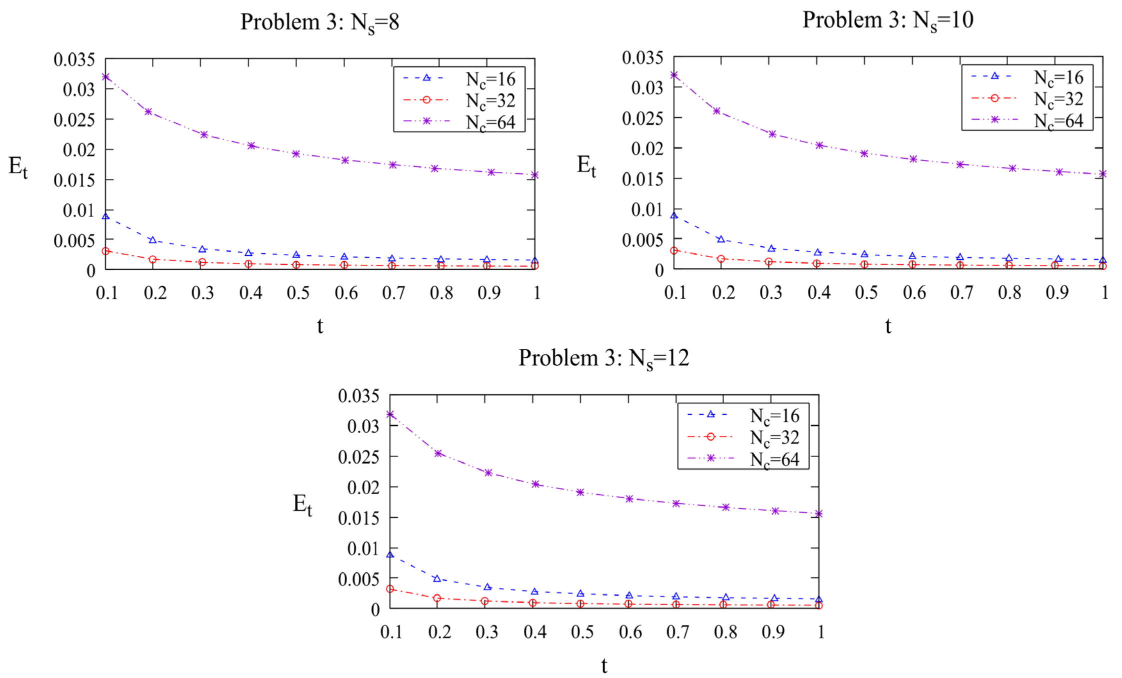

Fig. 15 *Values of E_t for Problem 3*

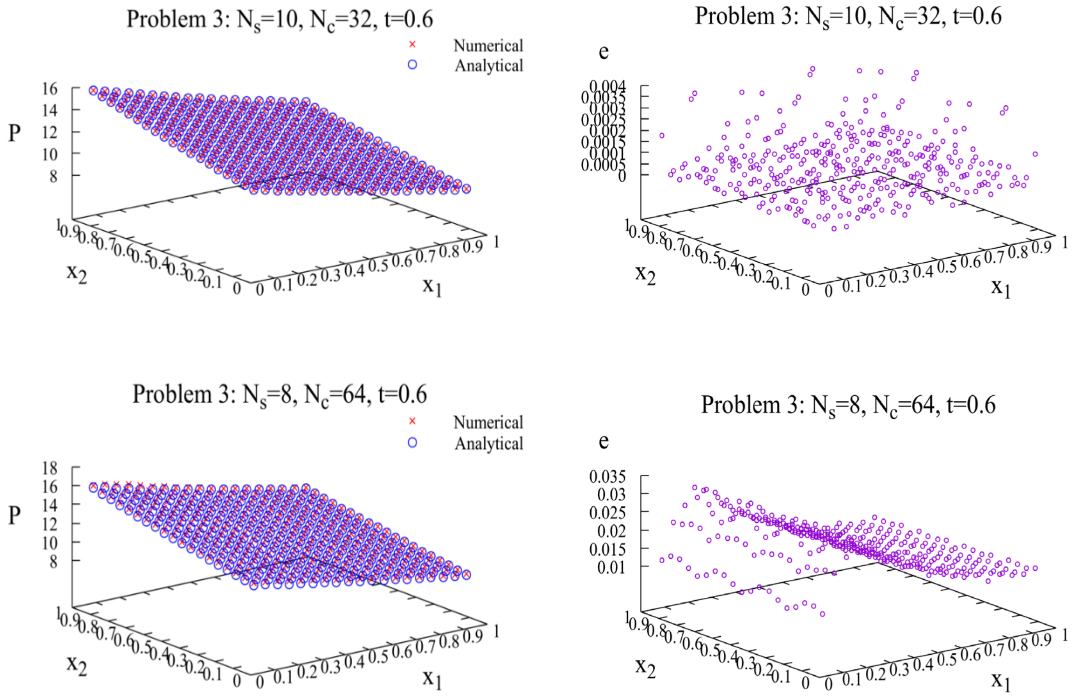

Fig. 16 *Values of P and e at t = 0.6 for Problem 3*

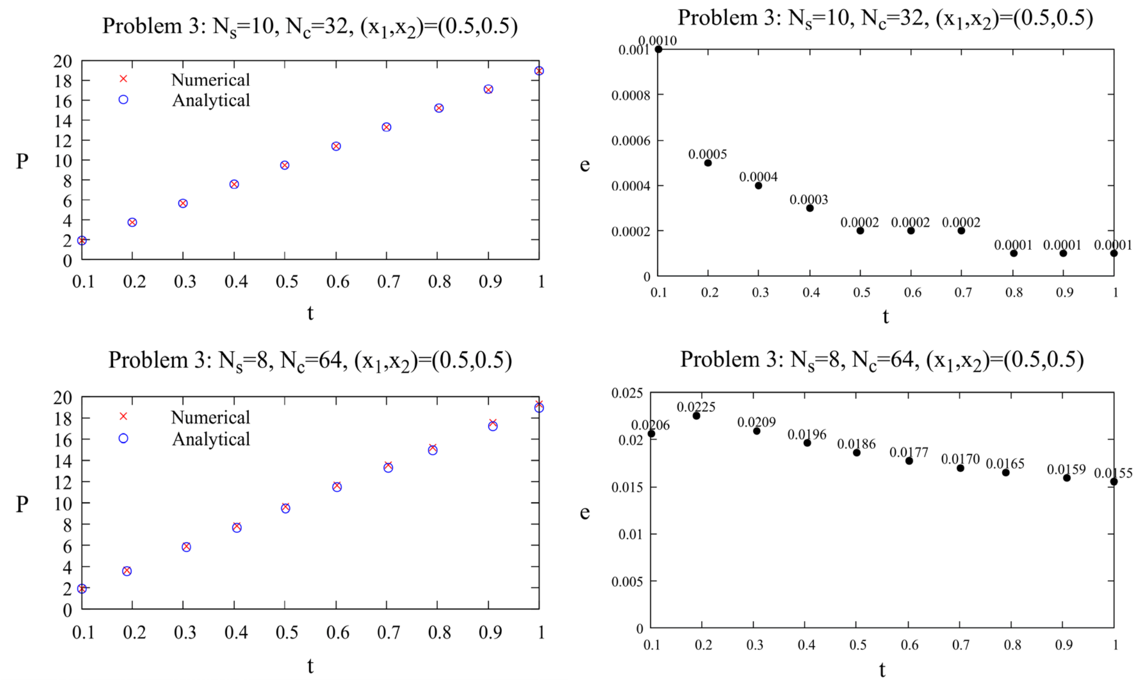

Fig. 17 *Values of P and e at (x_1,x_2)=(0.5,0.5) for Problem 3*

5. Conclusions

The combination of the DBEM with the LT has been utilized to compute numerical solutions for initial boundary value problems governed by the variable coefficient Helmholtz-type equation outlined in Eq. (1). Domain integrals were evaluated using quadrature over triangular cells, whereas the Stehfest formula was employed for the numerical inversion of LT. The LT-DBEM approach is both accurate and straightforward to implement, achieving mean absolute relative errors as low as E = 0.001138 for quadratic gradation materials, E = 0.003411 for exponential gradation materials, and E = 0.004279 for trigonometric gradation materials. The computational analysis shows relative CPU times ranging from θ = 0.302452s to θ = 1.93548s depending on the material gradation type and discretization parameters.

Unlike methods involving fundamental solutions dependent on the time variable t, which may introduce round-off errors owing to integration over t, the LT-DBEM computes solutions for Eq. (18) independently for each specific value of t for which a solution is required. Methods using time variable fundamental solutions may yield less accurate results owing to potential time singular points in the fundamental solution and the propagation of round-off errors from one time step to the next. The current approach demonstrates consistent accuracy maintained across the time interval $t \in [0.1, 1.0]$ for all material types studied.

The LT-DBEM has been successfully applied to a broader range of FGMs, including materials with quadratic, exponential, and trigonometric gradations taking the forms in Eq. (21). The study extends the method's capability to handle arbitrary source terms and initial conditions, making it applicable to more realistic acoustic wave problems in functionally graded materials with superior accuracy compared to existing approaches.

Acknowledgement

Communication of this research is made possible through monetary assistance by Universiti Tun Hussein Onn Malaysia and the UTHM Publisher's Office via Publication Fund E15216. This work was supported by Hasanuddin University with its TRG (Thematic Research Group) research fund of contract number 00518/UN4.22/PT.01.03/2025.

Conflict of Interest

The authors declare that there is no conflict of interest regarding the publication of the paper.

Author Contribution

*The authors confirm contribution to the paper as follows: **study conception and design:** Khaeruddin, Firman, Muh. Nur, Mohammad Ivan Azis; **data collection:** Khaeruddin, Firman, Muh. Nur, Mohammad Ivan Azis; **analysis and interpretation of results:** Khaeruddin, Firman, Muh. Nur, Mohammad Ivan Azis; **draft manuscript preparation:** Shahrul Azmir Osman, Eliza M. Yusup, Mohamad Nur Hidayat Mat, Mohammad Ivan Azis. Mohammad Ivan Azis reviewed the results and approved the final version of the manuscript.*

References

[1] Abdulla, Mohammed, Meftah Hrairi, Abdul Aabid, and Nur Azam Abdullah. " Finite Element Analysis of a Repaired Cracked Aluminium Plate with Piezoelectric Patches under Mechanical and Thermal Loading." *Journal of Advanced Research in Applied Sciences and Engineering Technology* 51, no. 1 (2025): 171-183. https://doi.org/10.37934/araset.51.1.171183

[2] Pornphol, Putsadee, Porpattama Hammachukiattikul, Emmanuel Sabastine, Rajarathinam Vadivel, and Saratha Sathasivam. " Modelling the Study of Hand, Foot and Mouth Disease Using SVEIQAR Derived Model." *Journal of Advanced Research in Applied Sciences and Engineering Technology* 47, no. 2 (2024): 193-212. https://doi.org/10.37934/araset.47.2.193212

[3] Sundaram, Indhira, and Srinivasa Raju Rallabandi. " Numerical Investigation of Diffusion thermo and Thermal Diffusion on Mixed Convection flow of Williamson Nanofluid through a vertical cone with porous material in the presence Thermal radiation and Activation Energy." *Journal of Advanced Research in Applied Sciences and Engineering Technology* 45, no. 2 (2025): 90-110. https://doi.org/10.37934/araset.45.2.90110

[4] Atiyah, Ayad, Yaser Alaiwi, Mohammed Hussein Radhi, and Ahmad Jundi. " Numerical analysis for enhanced water desalination in solar stills with optimized glass cover angles." *Journal of Advanced Research in Numerical Heat Transfer* 22, no. 1 (2024): 31-45. https://doi.org/10.37934/arnht.22.1.3145

[5] Triwibowo, Bayu, Haniif Prasetiawan, Ratna Dewi Kusumaningtyas, and Dewi Selvia Fardhyanti. " Modeling and Simulation of Drilling Gas Mixing Process with Various Conditions in Oil and Gas Pipeline Network." *Journal of Advanced Research in Numerical Heat Transfer* 21, no. 1 (2024): 39-52. https://doi.org/10.37934/arnht.21.1.3952

[6] Ab Rashid, Nik Muhammad Hafiz Nik, Abdul Aziz Hairuddin, Khairil Anas Md Rezali, Siti Ujila Masuri, Jamiluddin Jaafar, and Deni Fajar Fitriyana. " Computational Fluid Dynamics (CFD) Validation and Investigation the Effect of Piston Bowl Geometries Performance on Port Fuel Injection-Homogeneous Charge Compression Ignition (PFI-HCCI) Engines." *Journal of Advanced Research in Numerical Heat Transfer* 18, no. 1 (2024): 30-48. https://doi.org/10.37934/arnht.18.1.3048

[7] Azis, Moh Ivan. " Numerical solutions for the Helmholtz boundary value problems of anisotropic homogeneous media." *Journal of Computational Physics* 381 (2019): 42-51. https://doi.org/10.1016/j.jcp.2019.01.002

[8] Alfouneh, Mahmoud, Jinchen Ji, and Quantian Luo. "Damping design of harmonically excited flexible structures with graded materials to minimize sound pressure and radiation." *Engineering Optimization* 53, no. 2 (2021): 348-367. https://dx.doi.org/10.1080/0305215X.2020.1735381

[9] Qu, Yegao, and Guang Meng. "Prediction of acoustic radiation from functionally graded shells of revolution in light and heavy fluids." *Journal of Sound and Vibration* 376 (2016): 112-130. https://dx.doi.org/10.1016/j.jsv.2016.04.023

[10] Deng L-Y, Cao X-S, Ru Y. Asymptotic analytical solution of circumferential sh wave in functionally graded cylindrical shell and cylinder. Proceedings of the 15th Symposium on Piezoelectricity - Acoustic Waves and Device Applications - SPAWDA 2020, 2021, 103–107, 9445515. https://dx.doi.org/10.1109/SPAWDA51471.2021.9445515

[11] Napolitano, Marialuisa, Raffaele Dragonetti, and Rosario Romano. "A method to optimize the regenerator parameters of a thermoacoustic engine." *Energy Procedia* 126 (2017): 525-532. https://dx.doi.org/10.1016/j.egypro.2017.08.244

[12] Chen, Geng, Zhaoyu Li, Xinyan Li, Jingyuan Xu, Wenpeng Sun, Lihua Tang, and Zhibin Yu. "Optimal cross-sectional area ratio between porous material and resonance tube for the onset of self-excited oscillations in standing-wave thermoacoustic engines." *Thermal Science and Engineering Progress* 41 (2023): 101856. https://dx.doi.org/10.1016/j.tsep.2023.101856

[13] DOBRUCKI, Andrzej Bogdan, and K. R. U. K. Bartłomiej. "Influence of Working Conditions on Parameters of Thermoacoustic Engine with Travelling Wave." *Archives of Acoustics* 45, no. 3 (2020): 467-473. https://dx.doi.org/10.24425/aoa.2020.134063

[14] Azis, Moh Ivan. "A boundary integral investigation for unsteady modified Helmholtz problems of some other classes of anisotropic functionally graded materials." *International Journal of Computational Materials Science and Engineering* 10, no. 01 (2021): 2150005. https://doi.org/10.1142/S2047684121500056

[15] Wang, Chao, Fajie Wang, and Yanpeng Gong. "Analysis of 2D heat conduction in nonlinear functionally graded materials using a local semi-analytical meshless method." *Aims Math* 6, no. 11 (2021): 12599-12618. https://dx.doi.org/10.3934/MATH.2021726

[16] Azis, Moh Ivan, Mostafa Abbaszadeh, Mehdi Dehghan, and Imam Solekhudin. "A boundary-only integral equation method for parabolic problems of another class of anisotropic functionally graded materials." *Materials Today Communications* 26 (2021): 101956. https://doi.org/10.1016/j.mtcomm.2020.101956

[17] Azis, M. I. "An LT-BEM formulation for problems of anisotropic functionally graded materials governed by transient diffusion–convection–reaction equation." *Engineering Analysis with Boundary Elements* 135 (2022): 196-205. https://doi.org/10.1016/j.enganabound.2021.11.008

[18] Srivastava, Manish Chand, and Jeeoot Singh. "Assessment of RBFs Based Meshfree Method for the Vibration Response of FGM Rectangular Plate Using HSDT Model." *Mechanics Of Advanced Composite Structures* 10, no. 1 (2023): 137-150. https://doi.org/10.22075/macs.2022.27615.1418

[19] Kumar, Rahul, Anand Jain, Mahendra Singh, Jigyasa Singh, and Jeeoot Singh. "Porosity-dependent buckling analysis of elastically supported FGM sandwich plate via new tangent HSDT: A meshfree approach." *International Journal of Computational Materials Science and Engineering* 12, no. 01 (2023): 2250013. https://doi.org/10.1142/S2047684122500130

[20] Fouaidi, Mustapha, Kawtar Belfallah, Mohammad Jamal, and Naoual Belouaggadia. "Transient analysis of functionally graded graphene oxide powders-reinforced porous composite beams resting on elastic foundations using the reproducing kernel particle meshless method." *Engineering Analysis with Boundary Elements* 146 (2023): 460-472. https://doi.org/10.1016/j.enganabound.2022.10.029

[21] Azis, Moh Ivan, Mostafa Abbaszadeh, and Mehdi Dehghan. "An LT-BEM for an unsteady diffusion-convection problem of another class of anisotropic FGMs." *International Journal of Computer Mathematics* 99, no. 3 (2022): 575-590. https://doi.org/10.1080/00207160.2021.1925258

[22] Azis, Mohammad Ivan. "A numerical solution for unsteady anisotropic diffusion reaction equation of time–space variable coefficients." *Mathematical Methods in the Applied Sciences* 47, no. 3 (2024): 1628-1642. https://doi.org/10.1002/mma.9713

[23] Azis, Mohammad Ivan. "A combined BEM and Laplace transform for unsteady modified-Helmholtz equation of time–space variable coefficients for anisotropic media." *Engineering Computations* 40, no. 9/10 (2023): 3100-3115. https://doi.org/10.1108/EC-05-2023-0216

[24] Azis, Mohammad Ivan. "A numerical investigation of unsteady space–time dependent coefficients anisotropic-diffusion convection reaction equation." *Engineering Analysis with Boundary Elements* 155 (2023): 873-887. https://doi.org/10.1016/j.enganabound.2023.07.001